Cluster interpretation of properties of alternating parity bands in heavy nuclei

T. M. Shneidman,[1,2] G. G. Adamian,[1,2,3] N. V. Antonenko,[1,2] R. V. Jolos,[1,2] and W. Scheid[1]
[1]*Institut für Theoretische Physik der Justus-Liebig-Universität, D-35392 Giessen, Germany*
[2]*Joint Institute for Nuclear Research, RU-141980 Dubna, Russia*
[3]*Institute of Nuclear Physics, Tashkent 702132, Uzbekistan*
(Received 20 September 2002; published 22 January 2003)

The properties of the states of the alternating parity bands in actinides and Ba, Ce, and Nd isotopes are analyzed within a cluster model. The model is based on the assumption that cluster-type shapes are produced by the collective motion of the nuclear system in the mass asymmetry coordinate. The calculated spin dependences of the parity splitting and of the electric multipole transition moments are in agreement with the experimental data.

DOI: 10.1103/PhysRevC.67.014313 PACS number(s): 21.60.Ev, 21.60.Gx

I. INTRODUCTION

The low-lying negative parity states observed in actinides and in heaviest known Ba, Ce, Nd, and Sm isotopes are definitely related to reflection-asymmetric shapes [1,2]. There are several approaches to treat collective motion leading to reflection-asymmetric deformations. One of them is based on the concept of a nuclear mean field which has a static octupole deformation or is characterized by large amplitudes of reflection-asymmetric vibrations around the equilibrium shape [2–6]. In this approach the parity splitting is explained by octupole deformation. Another approach [7–10] is based on the assumption that the reflection-asymmetric shape is a consequence of alpha clustering in nuclei [11–13]. In the algebraic model [7–10] the corresponding wave functions of the ground and excited states consist of components without and with dipole bosons (in addition to the quadrupole bosons), which are related to mononucleus and alpha-cluster components, respectively. The variant of algebraic model including octupole bosons in addition to dipole bosons has been applied in [14,15] to the description of the low-lying negative parity states in actinides. In [16–19] a cluster configuration with a lighter cluster heavier than ^{4}He was used in order to describe the properties of the low-lying positive and negative parity states. In both models [7–10] and [16–19] the relative distance between the centers of mass of clusters at fixed mass asymmetry is the main collective coordinate for the description of the alternating parity bands.

Nuclear cluster effects are mostly pronounced in the light even-even $N=Z$ nuclei with the alpha particle as the natural building block. There is a nice relationship between the alpha-cluster description and deformed shell model [11]. It is known from Nilsson-Strutinsky-type calculations for light nuclei that nuclear configurations corresponding to the minima of the potential energy contain particular symmetries which are related to certain cluster structures [20–22]. By using an antisymmetrized molecular dynamics approach [23,24], the formation and dissolution of clusters in light nuclei, like ^{20}Ne and ^{24}Mg, are described. The idea of clusterization applied to heavy nuclei does not contradict the mean field approach. The coexistence of the clustering and of the mean field aspects is a unique feature of nuclear many body systems. The problem of the existence of a cluster structure in the ground state of heavy nuclei has attracted much attention, especially because of the experimentally observed cluster decay [25]. The available experimental and theoretical results provide evidence for existence of fission modes created by the clustering of fissioning nuclei [26]. Indications of clusterization of highly deformed nuclei are demonstrated in [27,28].

The aim of the present paper is a development of the cluster-type model which provides not only a qualitative but also a quantitative explanation of the properties of alternating parity bands. Descriptions of the excitation spectra, $E\lambda$-transition probabilities ($\lambda=1,2,3$), and the angular momentum dependence of the parity splitting [29,30] are the main subjects of this paper. Our model is based on the assumption that the reflection-asymmetric shapes are produced by the collective motion of the nuclear system in the mass asymmetry coordinate [31]. The values of the odd multipolarity transitional moments (dipole and octupole) are strongly correlated with the mass asymmetry deformation of nucleus. In general, the value of the quadrupole moment is related to the degree of the quadrupole correlations (deformation) in the nucleus. However, the collective motion in the mass asymmetry degree of freedom simultaneously creates a deformation with even and odd multipolarities. Therefore, calculations of $E\lambda$-transition moments are of interest in the proposed model. The single particle degrees of freedom are not taken explicitly into consideration since our aim is to show that the suggested cluster model gives a good quantitative explanation of the observed properties of the low-lying negative parity states. If it is so, this model can serve as a good ground for development of an extended model with additional degrees of freedom.

It should be noted that the first results of the calculations of the alternating parity spectra for a few actinides within the cluster model have been already presented in [31]. Besides Ra, Th, and U isotopes, in the present paper we present the results of calculations of the energies of alternating parity bands in ^{240,242}Pu, ^{144,146,148}Ba, ^{146,148}Ce, and ^{146,148}Nd. The electromagnetic transitions are described in this paper with the cluster model for many nuclei and the spin dependence of the intrinsic quadrupole transition moment is predicted for ^{238}U. Simple analytical expressions obtained for the par-

ity splitting and the spectra of alternating parity bands are useful for estimations. The dependence of alpha clusterization in actinides on the angular momentum is shown for the first time.

II. MODEL

A. Hamiltonian in mass asymmetry coordinate

Dinuclear systems consisting of a heavy cluster A_1 and a light cluster A_2 were first introduced to explain data on deep inelastic and fusion reactions with heavy ions [32–34]. The mass asymmetry coordinate η, defined as $\eta=(A_1-A_2)/(A_1+A_2)$ ($|\eta|=1$ if $A_1=0$ or $A_2=0$), which describes a partition of nucleons between the nuclei forming the dinuclear system, and the distance R between the centers of clusters, are used as relevant collective variables [35]. The wave function in η can be thought as a superposition of different cluster-type configurations including the mononucleus configuration with $|\eta|=1$, which are realized with certain probabilities. The relative contribution of each cluster component in the total wave function is determined by the collective Hamiltonian described below. Our calculations have shown that in the cases considered the dinuclear configuration with an alpha cluster ($\eta=\eta_\alpha$) has a potential energy which is close to or even smaller than the energy of the mononucleus at $|\eta|=1$ [28,31]. Since the energies of configurations with a light cluster heavier than an α particle increase rapidly with decreasing $|\eta|$, we restrict our investigations to configurations with light clusters not heavier than Li ($\eta=\eta_{Li}$), i.e., to cluster configurations near $|\eta|=1$.

The Hamiltonian describing the dynamics in η has the following form:

$$H=-\frac{\hbar^2}{2B_\eta}\frac{d^2}{d\eta^2}+U(\eta,I), \tag{1}$$

where B_η is the effective mass and $U(\eta,I)$ is the potential. In order to calculate the dependence of parity splitting on the angular momentum and the electric dipole, quadrupole, and octupole transition moments we search for solutions of the stationary Schrödinger equation describing the dynamics in η:

$$H\Psi_n(\eta,I)=E_n(I)\Psi_n(\eta,I). \tag{2}$$

The eigenfunctions Ψ_n of this Hamiltonian have a well-defined parity with respect to the reflection $\eta\rightarrow-\eta$. Before we come to the results of Eq. (2), we discuss the calculation of the potential $U(\eta,I)$, the mass parameter B_η, and the moments of inertia $\Im(\eta)$ appearing in H.

B. Potential energy

The potential $U(\eta,I)$ in Eq. (1) is taken as a dinuclear potential energy for $|\eta|<1$:

$$U(\eta,I)=B_1(\eta)+B_2(\eta)-B+V(R=R_m,\eta,I). \tag{3}$$

Here, the internuclear distance $R=R_m$ is the touching distance between the clusters and is set to be equal to the value corresponding to the minimum of the potential in R for a given η. The quantities B_1 and B_2 (which are negative) are the experimental binding energies of the clusters forming the dinuclear system at a given mass asymmetry η, and B is the binding energy of the mononucleus. The quantity $V(R,\eta,I)$ in Eq. (3) is the nucleus-nucleus interaction potential. It is given as

$$V(R,\eta,I)=V_{Coul}(R,\eta)+V_N(R,\eta)+V_{rot}(R,\eta,I), \tag{4}$$

with the Coulomb potential V_{Coul}, the centrifugal potential $V_{rot}=\hbar^2I(I+1)/[2\Im(\eta,R)]$, and the nuclear interaction V_N. In the realization of the cluster model developed in this paper, where the overlap of clusters is much smaller than in the model of [16], the choice of the relevant cluster configuration follows the minimum of the total potential energy of the system with a cluster-cluster interaction taken additionally into consideration. As a result we describe the same nuclear properties as in [16] with configurations of clusters having larger mass asymmetry and a smaller overlap.

The potential $V(R,\eta,I)$ and the moment of inertia $\Im(\eta,R)$ are calculated for special cluster configurations only, namely, for the mononucleus ($|\eta|=1$) and for the two cluster configurations with the α and Li clusters as light clusters, respectively. These calculated points are used later to interpolate the potential smoothly by a polynomial. The energies of the Li-cluster configurations are about 15 MeV larger than the binding energies of the mononuclei considered. Therefore, for small excitations only oscillations in η are of interest which lie in the vicinity of $|\eta|=1$, i.e., only cluster configurations up to Li clusters need to be considered. The potential V_N is obtained with a double folding procedure with the ground state nuclear densities of the clusters. Antisymmetrization between the nucleons belonging to different clusters is regarded by a density dependence of the nucleon-nucleon force which gives a repulsive core in the cluster-cluster interaction potential. Details of the calculation of V_N are given in [36]. The parameters of the nucleon-nucleon interaction are fixed in nuclear structure calculations [37]. Other details are presented in [31].

Our calculations show that the potential energy has a minimum at $|\eta|=\eta_\alpha$ in ^{218,220,222,224,226}Ra and ^{222,224,226}Th isotopes. In order to demonstrate the dependence of the potential on the neutron number, we present in Fig. 1 calculated values of $U(\eta_\alpha,I=0)\equiv U(\eta_\alpha)$ of configurations with an α cluster taking the long chain of Ba isotopes as an example. In the neutron deficient isotopes $U(\eta_\alpha)$ is smaller than zero and an α clusterization is more likely. When the neutron number approaches the magic value of 82, the nucleus becomes stiffer with respect to vibrations in η and $U(\eta_\alpha)$ is larger than zero. The appearance of two neutrons above shell closure is in favor of an α clusterization. In this case $U(\eta_\alpha)$ drops much and again becomes smaller than zero. Further addition of neutrons increases the nuclear stiffness with respect to η vibrations.

C. Moments of inertia

The calculation of the moment of inertia $\Im(\eta)=\Im(\eta,R_m)$ needed to determine the potential energy at

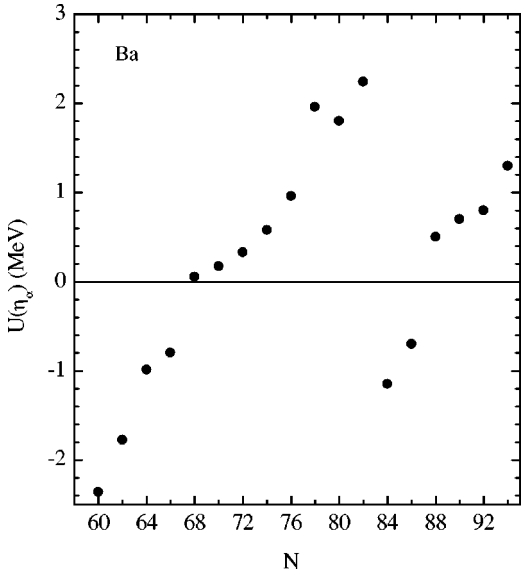

FIG. 1. Potential energy (solid circles) of the α-cluster configuration $U(\eta_\alpha) \equiv U(\eta_\alpha, I=0)$ as a function of the neutron number in Ba isotopes.

$I \neq 0$ has been described in [31]. For completeness, we repeat in this subsection the most important information. As was shown in [28], the highly deformed states are well described as cluster systems and their moments of inertia are about 85% of the rigid-body limit. Following this, we assume that the moment of inertia of the cluster configurations with α and Li as light clusters can be expressed as

$$\Im(\eta) = c_1 \left(\Im_1^r + \Im_2^r + m_0 \frac{A_1 A_2}{A} R_m^2 \right). \tag{5}$$

Here, $\Im_i^r$, $(i=1,2)$ are the rigid-body moments of inertia for the clusters of the dinuclear system, $c_1 = 0.85$ [28,31] for all considered nuclei, and m_0 is the nucleon mass.

It should be noted that the angular momentum is treated in this paper as the sum of the angular momentum of the collective rotation of the clusters and of the orbital momentum of the relative motion of the two clusters. Single particle effects, like alignment of the single particle angular momentum in the heavy cluster, are presently disregarded.

For $|\eta| = 1$, the value of the moment of inertia is not known from the data because the experimental moment of inertia is a mean value between the moment of inertia of the mononucleus ($|\eta| = 1$) and the ones of the cluster configurations arising due to the oscillations in η. We assume that

$$\Im(|\eta| = 1) = c_2 \Im^r(|\eta| = 1), \tag{6}$$

where $\Im^r$ is the rigid-body moment of inertia of the mononucleus with A nucleons calculated with deformation parameters from [38] and c_2 is a scaling parameter which is fixed by the energy of the first 2^+ or other positive parity states, for example, 6^+. The chosen values of c_2 vary in the interval $0.1 < c_2 < 0.3$. So in our calculations there is a free parameter c_2. However, this parameter is used to describe the rotational energies averaged over the parity and not the parity splitting studied in this paper.

D. Mass parameter

The method of the calculation of the inertia coefficient B_η used in this paper is given in [39]. Our calculations show that B_η is a smooth function of the mass number A. As a consequence, we take nearly the same value of $B_\eta = 20 \times 10^4 m_0$ fm^2 for almost all considered actinide nuclei with a variation of 10%. However, for ^{222}Th and ^{220,222}Ra we varied B_η in the range $B_\eta = (10\text{–}20) \times 10^4 m_0$ fm^2 to obtain the correct value of $E_0(I=0)$. These variations of B_η lead to better results for light Ra isotopes than those in [31], where the calculated values of the parity splitting at the beginning of the alternating parity band are smaller than the experimental ones. Using a smooth mass dependence of B_η [39] we get $B_\eta = 4.5 \times 10^4 m_0$ fm^2 in the Ba, Ce, and Nd regions. However, we obtain better results for $B_\eta = 3 \times 10^4 m_0$ fm^2.

For very asymmetric dinuclear systems, we can use simple analytical expressions to establish a connection between the relative distance and mass asymmetry coordinates on one side and the multipole expansion coefficients β_2 and β_3 on the other side [28]:

$$\beta_2 = \sqrt{\frac{5}{4\pi}} \frac{\pi}{3} (1-\eta^2) \frac{R^2}{R_0^2},$$

$$\beta_3 = \sqrt{\frac{7}{4\pi}} \frac{\pi}{3} \eta (1-\eta^2) \frac{R^3}{R_0^3}. \tag{7}$$

Here, R_0 is the spherical equivalent radius of the corresponding compound nucleus. One finds

$$\frac{d\beta_3}{d\eta} = \frac{\sqrt{7\pi}}{12} [(1+\eta)^{1/3} + (1-\eta)^{1/3}]^3 \times \left[(1-3\eta^2) + \eta(1-\eta^2) \frac{(1+\eta)^{-2/3} - (1-\eta)^{-2/3}}{(1+\eta)^{1/3} + (1-\eta)^{1/3}} \right]. \tag{8}$$

In the actinide region for an α-particle configuration, $\eta \approx 0.96$ and $(d\beta_3/d\eta)^2 \approx 11.25$. Then the mass parameters for β_3 and η variables are related as

$$B_\eta \approx (d\beta_3/d\eta)^2 B_{\beta_3}. \tag{9}$$

If we take the value of $B_{\beta_3} = 200\hbar^2$ MeV^{-1} known from the literature [4], then $B_\eta \approx 9.3 \times 10^4 m_0$ fm^2. This value is compatible with the one used in our calculations.

III. INTRINSIC ELECTRIC MULTIPOLE MOMENTS

Solving the eigenvalue equation (2), we obtain the wave functions of the positive and negative parity states for different values of the quantum number I of the angular momentum. These wave functions are used then to calculate transi-

tion matrix elements of the electric multipole operators by integration over η. The electric multipole operators for a system of a dinuclear shape have been calculated [28] by using the following expression:

$$Q_{\lambda\mu}=\sqrt{\frac{16\pi}{2\lambda+1}}\int \rho^{Z}(\mathbf{r})r^{\lambda}Y_{\lambda\mu}(\Omega)d\tau. \tag{10}$$

For slightly overlapping clusters when the intercluster distance R_m is about or larger than the sum of the radii of clusters (R_1+R_2), the nuclear charge density ρ^Z can be taken as a sum of the cluster charge densities:

$$\rho^{Z}(\mathbf{r})=\rho_1^{Z}(\mathbf{r})+\rho_2^{Z}(\mathbf{r}). \tag{11}$$

Using Eq. (11) and assuming axial symmetry of the nuclear shape, we obtain [28] the following expressions for the intrinsic electric multipole moments:

$$Q_{10}=2D_{10}=e\frac{A}{2}(1-\eta^2)R_m\left(\frac{Z_1}{A_1}-\frac{Z_2}{A_2}\right), \tag{12}$$

$$Q_{20}=e\frac{A}{4}(1-\eta^2)R_m^2\left((1-\eta)\frac{Z_1}{A_1}+(1+\eta)\frac{Z_2}{A_2}\right)+Q_{20}(1)+Q_{20}(2), \tag{13}$$

$$Q_{30}=e\frac{A}{8}(1-\eta^2)R_m^3\left((1-\eta)^2\frac{Z_1}{A_1}-(1+\eta)^2\frac{Z_2}{A_2}\right)+\frac{3}{2}R_m[(1-\eta)^2Q_{20}(1)-(1+\eta)^2Q_{20}(2)], \tag{14}$$

where the charge quadrupole moments of clusters $Q_{20}(i)(i=1,2)$ are calculated with respect to their centers of mass. Effective charges for electric dipole and octupole transitions are used in our calculations in order to take the coupling of the mass asymmetry mode to the higher-lying giant dipole and octupole excitations [40] effectively into account, which are not present in the model.

The charge to mass ratios Z_1/A_1 and Z_2/A_2 are functions of η. For instance, for $|\eta|=1$ (mononucleus) this ratio takes the values 0.3–0.4 for the nuclei considered in the paper. For the α particle this ratio is equal to 0.5. The results for the electric dipole moment are sensitive to the dependence of Z/A on η. In the calculations we parametrize the Z_i/A_i ratio in the following way. For $\eta_\alpha<|\eta|\leqslant 1$, the ratio Z_2/A_2 for the light cluster takes the same value as for the mononucleus. For a smaller value of $|\eta|$, we set it equal to 0.5 as for the α cluster.

IV. RESULTS OF THE CALCULATIONS AND DISCUSSION

A. Calculation procedure

As was mentioned in Sect. II B, our consideration can be restricted to cluster configurations near $|\eta|=1$. Then it is convenient to substitute the coordinate η by the variable

$$x=\eta-1 \quad \text{if} \quad \eta>0,$$

$$x=\eta+1 \quad \text{if} \quad \eta\leqslant 0,$$

and to use the smooth parametrization

$$U(x,I)=\sum_{k=0}^{4} a_{2k}(I)x^{2k} \tag{15}$$

of the potential $U(\eta,I)$ from Eq. (3). This formula contains five parameters $a_{2k}(I)$. If a minimum of the potential is located at $|x|=x_\alpha$, four parameters are determined by the experimental ground state energy, potential energies $U(x,I)$ for $x=x_\alpha$, $x=x_{Li}$, and by the requirement that the potential has a minimum at $|x|=x_\alpha$. The fifth parameter a_8 is necessary to avoid a falloff of the potential for $|x|\geqslant x_{Li}$ because of the negative value of a_6 needed to describe correctly $U(x_{Li},I)$. We take the minimal necessary positive value of a_8 to guarantee an increase of U for $|x|>x_{Li}$. The ground state energy is obtained by solving the Schrödinger equation. Since the ground state wave function is distributed over x, the potential energy at $x=0$ is not equal to the experimental binding energy of the mononucleus. To reach the correct value of the ground state energy $E_0(I=0)=0$, we can vary the potential $U(x=0, I=0)$. In the majority of cases this procedure leads to a value of $U(x=0, I=0)$ close to $E_0(I=0)$. The variation of B_η is also done in the case of light Ra isotopes to obtain $E_0(I=0)=0$. Besides the barrier height, which determines the stiffness of the potential well at $x=x_\alpha$, the ground state energy $E_0(I=0)$ of Eq. (2) depends also on the frequency of oscillations in x. This frequency is ruled by the value of the inertia coefficient B_η. If the minimum is located at $x=0$ $(|\eta|=1)$, only three parameters a_0, a_2, and a_4 in Eq. (15) are necessary. Potentials with other parametrizations show almost no difference in the description of the parity splitting in the majority of considered nuclei.

B. Parity splitting

With Eq. (2) we first calculated the parity splitting for the isotopes of Ra, Th, U, Pu, Ba, Ce, and Nd for different values of the angular momentum I. The results of calculations are shown in Tables I–V. As is seen from the tables, they agree well with the experimental data [41–49,52]. The largest deviations of the calculated values from the experimental ones are found at low spins in some of the considered nuclei. A good description of the experimental data, especially of the variation of the parity splitting with A at low I and of the value of the critical angular momentum at which the parity splitting disappears, means that the dependence of the potential energy on η and I for the considered nuclei is described correctly by the proposed cluster model. The used value of the inertia coefficient B_η is also important.

Of course, other effects related to the degrees of freedom, which are not included in the model, like the alignment of the single particle momenta or interaction with other negative parity bands with different K quantum number, can contribute as well. However, a general agreement between the experimental data and the results of calculations shows that

TABLE I. Comparison of experimental (E_{expt}) and calculated (E_{calc}) energies of states of the alternating parity bands in $^{232-222}$Th. Energies are given in keV. Experimental data are taken from [41,42].

	^{232}Th		^{230}Th		^{228}Th		^{226}Th		^{224}Th		^{222}Th	
I^π	E_{expt}	E_{calc}	E_{expt}	E_{calc}	E_{expt}	E_{calc}	E_{expt}	E_{calc}	E_{expt}	E_{calc}	E_{expt}	E_{calc}
1^-	714	693	508	485	328	350	230	254	251	204	250	195
2^+	49	49	53	53	58	58	72	72	98	98	183	183
3^-	774	761	572	557	396	423	308	340	305	311	467	366
4^+	162	160	174	172	187	177	226	238	284	296	440	461
5^-	884	882	687	684	519	549	451	490	465	494	651	616
6^+	333	330	357	354	378	391	447	475	535	563	750	760
7^-	1043	1051	852	859	695	748	658	698	700	739	924	920
8^+	557	553	594	589	623	634	722	761	834	868	1094	1077
9^-	1249	1263	1065	1075	921	971	923	958	998	1036	1255	1258
10^+	827	822	880	869	912	919	1040	1079	1174	1202	1461	1430
11^-	1499	1511	1322	1326	1190	1229	1238	1263	1347	1384	1623	1624
12^+	1137	1130	1208	1215	1239	1235	1395	1424	1550	1564	1851	1815
13^-	1785	1792	1615	1629	1497	1517	1596	1609	1739	1772	2016	2019
14^+	1482	1470	1573	1565	1605	1572	1781	1796	1959	1966	2260	2226
15^-	2101	2099	1946	1941	1838	1823	1989	2002	2165	2194	2432	2450
16^+	1858	1841	1971	1935	1993	1918	2196	2200	2398	2405	2688	2663
17^-	2445	2449	2310	2274	2209	2154	2413	2429	2620	2651	2873	2906
18^+	2262	2229	2398	2318	2406	2281	2635	2640	2864	2880	3134	3128
19^-	2813	2794	2703	2624			2861	2890			3341	3380
20^+	2691	2633	2850	2709			3097	3115			3596	3621

TABLE II. Comparison of experimental (E_{expt}) and calculated (E_{calc}) energies of states of the alternating parity bands in $^{220-226}$Ra and ^{240,242}Pu. Energies are given in keV. Experimental data are taken from [41–43]. For ^{220,222}Ra, the parameter c_2 was adjusted to the 6^+ state.

	^{226}Ra		^{224}Ra		^{222}Ra		^{220}Ra		^{242}Pu		^{240}Pu	
I^π	E_{expt}	E_{calc}	E_{expt}	E_{calc}	E_{expt}	E_{calc}	E_{expt}	E_{calc}	E_{expt}	E_{calc}	E_{expt}	E_{calc}
1^-	254	254	216	193	242	224	413	385	781	778	597	597
2^+	68	68	85	85	111	96	179	125	45	45	43	43
3^-	322	327	291	282	317	324	474	509	832	843	649	659
4^+	212	206	251	253	302	287	410	375	147	146	142	142
5^-	447	455	433	434	474	486	635	709	927	958	742	774
6^+	417	414	480	482	550	550	688	688	306	304	294	295
7^-	627	635	641	642	703	728	873	962		1122		945
8^+	670	668	756	747	843	843	1001	1016	518	514	498	499
9^-	858	862	907	901	992	1014	1164	1252		1329		1145
10^+	960	954	1069	1046	1173	1166	1343	1356	779	773	748	750
11^-	1134	1134	1222	1215	1331	1346	1496	1568		1578		1392
12^+	1282	1270	1415	1378	1537	1525	1711	1706	1084	1077	1042	1044
13^-	1448	1449	1578	1558	1710	1722	1864	1904		1863		1677
14^+	1629	1621	1789	1745	1933	1924	2106	2067	1431	1421	1376	1377
15^-	1797	1810	1970	1944	2125	2140	2263	2257		2181		1994
16^+	1999	2003	2189	2153	2359	2366			1816	1800		
17^-	2175	2220	2389	2372	2570	2602				2526		
18^+									2236	2210		
19^-										2894		
20^+									2686	2646		

TABLE III. Comparison of experimental (E_{expt}) and calculated (E_{calc}) energies of states of the alternating parity bands in $^{238-232}$U. Energies are given in keV. Experimental data are taken from [41].

	^{238}U		^{236}U		^{234}U		^{232}U	
I^π	E_{expt}	E_{calc}	E_{expt}	E_{calc}	E_{expt}	E_{calc}	E_{expt}	E_{calc}
1^-	680	675	688	644	786	778	563	583
2^+	45	45	45	45	44	44	48	48
3^-	732	744	744	713	849	846	629	653
4^+	148	156	150	154	143	155	157	158
5^-	827	863	848	831	963	963	747	774
6^+	307	316	310	313	296	314	323	320
7^-	966	1025	1000	992	1125	1122	915	938
8^+	518	520	522	516	497	517	541	527
9^-	1150	1222	1199	1189	1336	1316	1131	1138
10^+	776	759	782	753	741	754	806	768
11^-	1378	1448					1391	1366
12^+	1077	1025					1112	1036

the simple cluster model used in this paper gives firm grounds for the consideration of the alternating parity bands.

In the considered nuclei the ground state energy level lies near the top of the barrier in η, if exists, and the weight of the α-cluster configuration (Fig. 2) estimated as that contribution to the norm of the wave function which is located at $|\eta| \leqslant \eta_\alpha$ is about 5×10^{-2} for ^{226}Ra, which is close to the calculated spectroscopic factor [25]. This means that our model is in qualitative agreement with the known α-decay widths of the nuclei considered.

The spectra of those considered nuclei whose potential energy has a minimum at the alpha-cluster configuration can be well approximated by the following analytical expressions:

$$E(I)=\frac{\hbar^2}{2J(I)}I[I+1], \quad \text{if} \quad I \quad \text{is even},$$

$$E(I)=\frac{\hbar^2}{2J(I)}I[I+1]+\delta E(I), \quad \text{if} \quad I \quad \text{is odd.} \quad (16)$$

Here the parity splitting $\delta E(I)$ is given as

$$\delta E(I)=\frac{2E_1(I^\pi=1^-)}{1+\exp(b_0\sqrt{B_0 I[I+1]})}, \quad (17)$$

with

TABLE IV. Comparison of experimental (E_{expt}) and calculated (E_{calc}) energies of states of the ground state alternating parity bands in $^{144-148}$Ba. Energies are given in keV. Experimental data are taken from [41,44]. The parameter c_2 was adjusted to the 6^+ state.

	^{148}Ba		^{146}Ba		^{144}Ba	
I^π	E_{expt}	E_{calc}	E_{expt}	E_{calc}	E_{expt}	E_{calc}
1^-		623	739	664	759	607
2^+	142	124	181	143	199	157
3^-	775	771	821	818	838	763
4^+	423	400	514	469	530	505
5^-	963	1018	1025	1078	1039	1026
6^+	808	808	958	958	961	961
7^-	1256	1342	1349	1424	1355	1375
8^+	1265	1273	1483	1491	1471	1496
9^-	1645	1731	1778	1841	1772	1796
10^+	1768	1788	2052	2028	2044	2005
11^-	2117	2181	2293	2323	2278	2285
12^+	2304	2327	2632	2574	2667	2546
13^-			2877	2871	2863	2843
14^+			3193	3166	3321	3146
15^-			3524	3489	3519	3473
16^+			3737	3823	3992	3815
17^-					4242	4179

TABLE V. Comparison of experimental (E_{expt}) and calculated (E_{calc}) energies of states of the ground state alternating parity bands in ^{146,148}Ce and ^{146,148}Nd isotopes. Energies are given in keV. Experimental data are taken from [41,45–49]. The parameter c_2 was adjusted to the 6^+ state.

	^{148}Ce		^{146}Ce		^{148}Nd		^{146}Nd	
I^π	E_{expt}	E_{calc}	E_{expt}	E_{calc}	E_{expt}	E_{calc}	E_{expt}	E_{calc}
1^-	760	714	925	776	1023	734		896
2^+	159	134	259	195	302	279	454	327
3^-	841	851	961	956	999	943	1190	1202
4^+	453	424	668	614	752	776	1042	993
5^-		1084	1183	1259	1242	1261	1518	1684
6^+	840	840	1171	1171	1280	1280	1780	1780
7^-		1400	1550	1660	1645	1647	2029	2264
8^+	1290	1289	1737	1756	1856	1788	2594	2510
9^-		1790	2019	2138	2132	2084	2706	2889
10^+	1792	1793	2552	2345	2472	2286	3320	3195
11^-		2246	2562	2681	2677	2573	3501	3544
12^+	2328	2334	3013	2953	3107	2819	3998	3879
13^-		2769	3163	3286	3265	3120	4295	4235
14^+	2888	2919		3603			4694	4594
15^-		3358	3827	3954			5058	4970
16^+	3464	3554					5461	5356
17^-		4013						
18^+	4065	4243						
19^-		4735						
20^+	4685	4983						

$$B_0=\frac{\hbar^2}{2}\left(\frac{1}{\Im(\eta=1)}-\frac{1}{\Im(\eta=\eta_\alpha)}\right).$$

The quantity B_0 describes the change of the height of the barrier with spin I. The moment of inertia in Eq. (16) is given by the expression

$$J(I)=w_m(I)\Im(\eta=1)+[1-w_m(I)]\Im(\eta=\eta_\alpha), \quad (18)$$

containing a weight function $w_m(I)$,

$$w_m(I)=\frac{w_m(I=0)}{1+b_1B_0I[I+1]}, \quad (19)$$

which is the probability to find the mononucleus component in the wave function of the state with spin I of the ground state band. Since $w_m(I)$ decreases with increasing angular momentum, $J(I)$ increases with I in agreement with the experimental tendency. The quantity $w_\alpha(I)=1-w_m(I)$ gives the corresponding probability of the α-cluster component. A qualitative derivation of the above analytical formulas is given in the Appendix. The constants $\Im(|\eta|=1)=0.3\times\Im^r(|\eta|=1)$, $w_m(I=0)=0.93$, $b_0=\pi$ MeV$^{-1/2}$, and $b_1=0.2$ MeV^{-1} were obtained by fitting the experimental spectra for the nuclei considered (see Fig. 3).

These formulas clearly demonstrate that there are two important quantities which predetermine a description of the spectra of the alternating parity bands. They are $E_1(I^\pi=1^-)$, which is determined by the depth of the minimum of the potential at $I=0$ and by the value of the mass parameter B_η, and B_0, which determines the angular momentum dependence of $\delta E(I)$ and $W_m(I)$, i.e., of $J(I)$.

C. $E\lambda$ transitions

With the wave functions obtained, we have calculated the reduced matrix elements of the electric multipole moments $Q(E1)$, $Q(E2)$, and $Q(E3)$. The effective charge for $E1$ transitions has been taken to be equal to $e_1^{eff}=e(1+\chi)$ with an average state-independent value of the $E1$ polarizability coefficient $\chi=-0.7$ [40]. This renormalization takes into account a coupling of the mass-asymmetry mode to the giant dipole resonance in a dinuclear system. In the case of the quadrupole transitions we did not renormalize the charge $e_2^{eff}=e$ although an effective charge of $1.35e$ describes the data for actinides better as is seen from the results of calculations. For octupole transitions our cluster model Hamiltonian includes the octupole mode responsible for the description of the shape variation and deformation of the nuclear surface. This is the low-frequency collective octupole mode. However, high-frequency isovector as well as isoscalar octupole modes are not present in the model Hamiltonian. For example, to simplify the consideration the charge asymmetry coordinate is not an independent dynamical one but is rigidly related in our model to the mass asymmetry coordinate. The octupole transition operator is not exhausted by the term produced by the low-frequency octupole degree of freedom and includes also a contribution of the high-frequency octupole modes. For this reason for the octupole transitions the effect of the coupling of the low-frequency

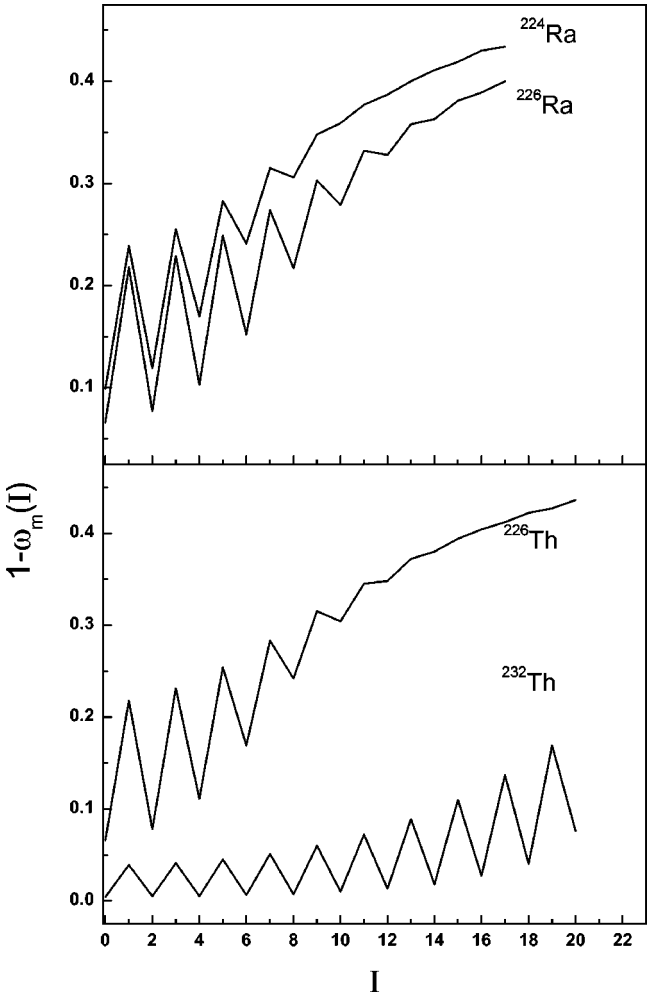

FIG. 2. Calculated probability of the α-cluster component in the wave function of the state with spin I of the alternating parity bands for ^{224,226}Ra and ^{226,232}Th.

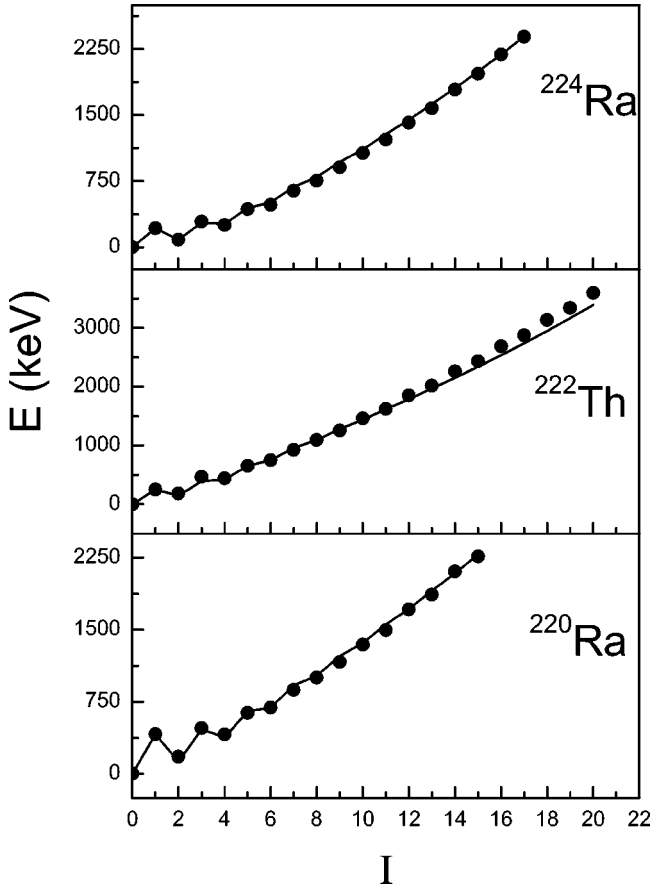

FIG. 3. Comparison of experimental (solid points) and calculated with Eqs. (16)–(19) (solid lines) energies of states of the alternating parity bands in ^{220,224}Ra and ^{222}Th. The fitting parameters are the same for all nuclei (see text). Experimental data are taken from [41,42].

octupole mode to the high frequency mode should be taken into account by the octupole effective charge. The estimate of this effective charge is given in [40]. The combined effect gives $\delta e_3^{(pol)} \approx (0.5+0.3\tau_z)e$ [40]. So we have taken the effective charge to be equal to $e^{eff}_{3,proton}=1.2e$ for protons and $e^{eff}_{3,neutron}=0.8e$ for neutrons.

The results of these calculations are listed in Tables VI and VII and shown in Figs. 4–10. The obtained values are in agreement with the known experimental data for Q_λ^{exp} [2,42,44–53]. Only in ^{224}Ra and ^{146}Ba (for $I=7$) the calculated values of D_{10} are larger by factor of 4 than the experimental D_{10}. In Th the isotopic dependence of the dipole moment is well reproduced. The higher multipole moments are in agreement with the calculations of Ref. [38]. Taking into account the collective character of our model and the absence of the parameters to fit the data, the description of the experimental data is rather good. It should be also noted that the experimental data of the dipole moment have some uncertainties.

The angular momentum dependence of the reduced matrix elements of the electric dipole operator is presented in Figs. 4 and 7 for ^{226}Ra and ^{148}Nd, respectively. The calculations qualitatively reproduce the angular momentum dependence of the experimental matrix elements [45,52]. The same is true for the reduced matrix elements of the electric quadrupole and octupole operators (Figs. 5, 6 and 8, 9).

Figure 10 illustrates the angular momentum dependence of the calculated intrinsic transition quadrupole moment. It is interesting that the cluster model shows an increase of the quadrupole moment with angular momentum in the transitional nucleus ^{226}Ra and a constant dependence in the well-deformed isotope ^{238}U. The staggering shown in Fig. 10 for both ^{226}Ra and ^{238}U nuclei is explained by the higher weight of the α-cluster component in the wave functions of odd I states (see Fig. 2). This cluster configuration has larger quadrupole and octupole deformations.

The calculated results for the $E3$-reduced matrix elements in ^{148}Nd exceed the experimental data for transitions to the ground band [45]. This can be explained as follows. The experimental $E3$ matrix elements connecting the negative parity states of ^{148}Nd to the β band are unexpectedly large, about 70% of the matrix elements within the ground state band [54]. This shows a considerable fractionation of the $E3$ strength among the $K=0$ bands. In our model the β degree of freedom is absent and all the $E3$ strength is concentrated in the transitions to the ground state band. The nucleus ^{148}Nd is transitional in its collective properties between spherical and deformed nuclei and the β anharmonicity is quite large.

TABLE VI. Calculated and experimental intrinsic multipole transition moments. The values of the dipole moment D_{10} are given for those values of the nuclear spin I for which there are experimental data. These values of I are shown in the second column. The experimental data are taken from [2,41–43,52,53].

Nucleus	D_{10} (e fm) Calc.	D_{10} (e fm) Expt.	$Q_{20}(0^+\rightarrow 2^+)$ (e fm^2) Calc.	$Q_{20}(0^+\rightarrow 2^+)$ (e fm^2) Expt.	$Q_{30}(0^+\rightarrow 3^-)$ (e fm^3) Calc.	$Q_{30}(0^+\rightarrow 3^-)$ (e fm^3) Expt.
^{220}Ra	0.28 ($I=7$)	0.27	397	558	3167	
^{222}Ra	0.30 ($I=7$)	0.27	395	675	3064	
^{224}Ra	0.133 ($I=3$)	0.028	510	633	2889	
^{226}Ra	0.111 ($I=1$)	0.06–0.10	574	718	2611	2861
^{222}Th	0.29 ($I=6$)	0.38	397	548	3632	
^{224}Th	0.312 ($I=10$)	0.52	495		2985	
^{226}Th	0.223 ($I=8$)	0.30	561	830	2672	
^{228}Th	0.151 ($I=8$)	0.12	653	843	2255	
^{230}Th	0.054 ($I=6$)	0.04	666	899	1935	2144
^{232}Th	0.007 ($I=1$)		719	966	1616	1969
^{234}U	0.004 ($I=1$)		758	1035	1541	1895
^{236}U	0.004 ($I=1$)		786	1080	1433	1951
^{238}U	0.004 ($I=1$)		818	1102	1417	2041

This explains a fractionation of the $E3$ strength between the ground state and the β bands. The summed $E3$ strength for ^{148}Nd corresponds to an intrinsic transitional octupole moment of $\sim 2000e$ fm^3 (instead of $\sim 1500e$ fm^3 for the transitions in the ground state band) which agrees with the calculated value.

V. SUMMARY

We suggest a cluster interpretation of the properties of the alternating parity bands in heavy nuclei assuming collective oscillations in the mass asymmetry degree of freedom. The existing experimental data on the angular momentum dependence of parity splitting and on multipole transition moments are quite well reproduced. This supports the idea that cluster-type states exist in heavy nuclei. The characteristics of the Hamiltonian used in the calculations were determined by investigating a completely different phenomenon, namely, heavy ion reactions at low energies. As a result of this fact, the predictive power of the suggested model is quite high. The proposed analytical expression (16) for $E(I)$ can be applied to estimate the position of the low-lying states which are not yet measured. The calculated staggering behavior of alpha clusterization can be verified by measuring the angular momentum dependence of the width of the alpha decay.

ACKNOWLEDGMENTS

T.M.S. and R.V.J. are grateful to BMBF and DFG (Bonn), respectively, for support. This work was supported in part by

TABLE VII. Calculated and experimental intrinsic multipole transition moments for Ba, Ce and Nd isotopes. The values of the dipole moment D_{10} are given for those values of the nuclear spin I for which there are experimental data. These values of I are shown in the second column. The experimental data are taken from [44–51].

Nucleus	D_{10} (e fm) Calc.	D_{10} (e fm) Expt.	$Q_{20}(0^+\rightarrow 2^+)$ (e fm^2) Calc.	$Q_{20}(0^+\rightarrow 2^+)$ (e fm^2) Expt.	$Q_{30}(0^+\rightarrow 3^-)$ (e fm^3) Calc.	$Q_{30}(0^+\rightarrow 3^-)$ (e fm^3) Expt.
^{144}Ba	0.194 ($I=7$)	0.071(10)	250	321	1295	
	0.209 ($I=8$)	0.14(3)				
^{146}Ba	0.055 ($I=3$)	0.06(4)	286	368	1147	
	0.170 ($I=7$)	0.037(3)				
^{148}Ba	0.095 ($I=7$)		306		938	
^{146}Ce	0.121 ($I=7$)	0.11(2)	313	305	1669	
^{146}Ce	0.160 ($I=11$)	0.20(2)				
^{148}Ce	0.152 ($I=7$)		364	436	1771	
^{146}Nd	0.071 ($I=11$)	0.17(2)	264	276	1627	
^{148}Nd	0.115 ($I=1$)	0.24(6)	370	400	2161	1500
	0.222 ($I=8$)	0.24(3)				

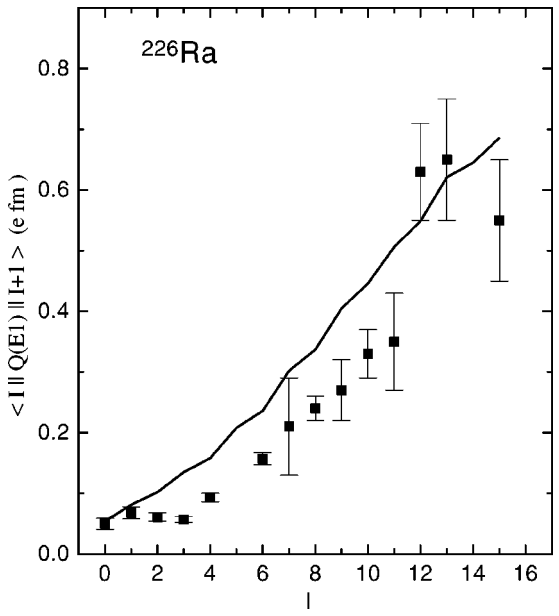

FIG. 4. Angular momentum dependence of the calculated reduced matrix elements of the electric dipole operator (solid curve) in ^{226}Ra. The experimental data (squares) are taken from [52].

Volkswagen-Stiftung (Hannover) and RFBR (Moscow). The support of STCU(Uzb-45), SCST, and UFBR (Tashkent) is acknowledged as well.

APPENDIX

Let us assume that the barrier at $x=0$ separates two minima of the potential (3): the minimum with reflection-asymmetric deformation (minimum of the potential at $x=x_\alpha$) and its mirror image. The nonzero penetration through this barrier lowers the energy of the levels with even I with respect to the energy of the levels with odd I. With increasing spin I the barrier between two minima, which is equal to $U_b(I)=U_b(I=0)+B_0 I[I+1]$, becomes higher and the penetration probability goes to zero. According to standard WKB analysis (with higher-order corrections) the transmission probability (per tunneling event) for the potential barrier described by the inverted oscillator with frequency $\hbar\omega_b(I)$ for the energy $\hbar\omega_m(I)/2$ above the potential minimum is given by [55]

$$P(I)=\frac{1}{1+\exp\left(2\pi\dfrac{U_b(I)-\hbar\omega_m(I)/2}{\hbar\omega_b(I)}\right)}, \qquad \text{(A1)}$$

and $\hbar\omega_b(I)\sim\sqrt{U_b(I)}$ at fixed x_α. Here, $\omega_m(I)$ is the frequency of the harmonic oscillator which approximates the potential U around the α-cluster minimum. Within the semiclassical approximation one can neglect the I dependence of ω_m, taking $\omega_m(I)\approx\omega_m(I=0)$. This frequency then essentially determines the rate ω_m/π at which the wave packet

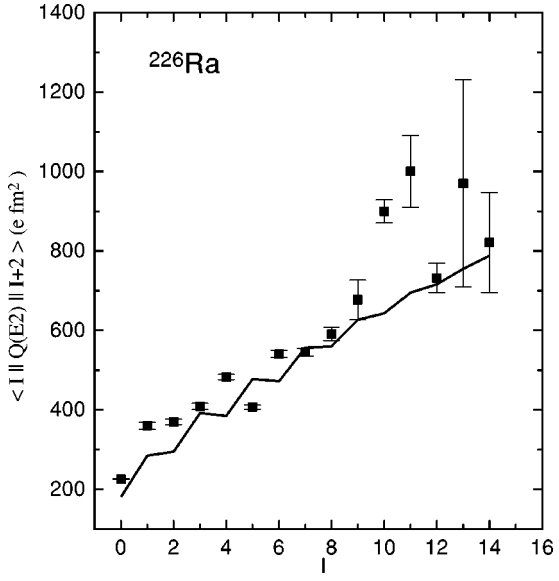

FIG. 5. The same as in Fig. 4, but for the quadrupole operator.

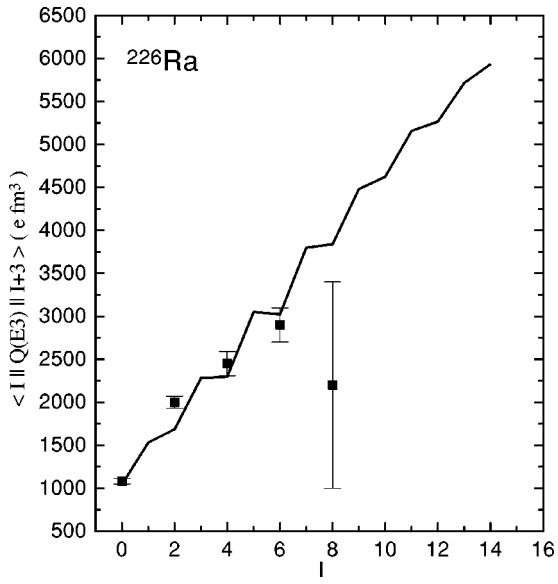

FIG. 6. The same as in Fig. 4, but for the octupole operator.

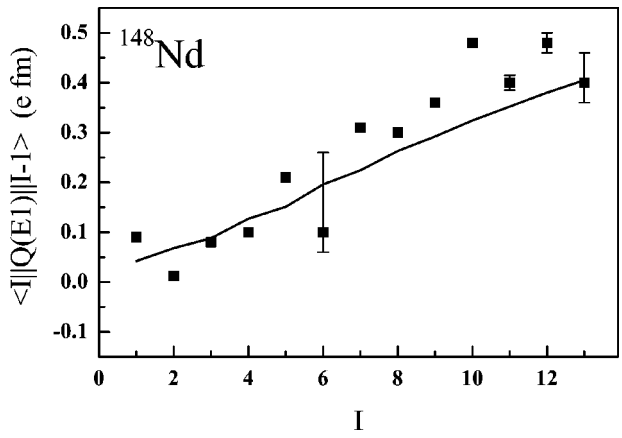

FIG. 7. Angular momentum dependence of the calculated reduced matrix elements of the electric dipole operator (solid curve) in ^{148}Nd. The experimental data (squares) are taken from [45].

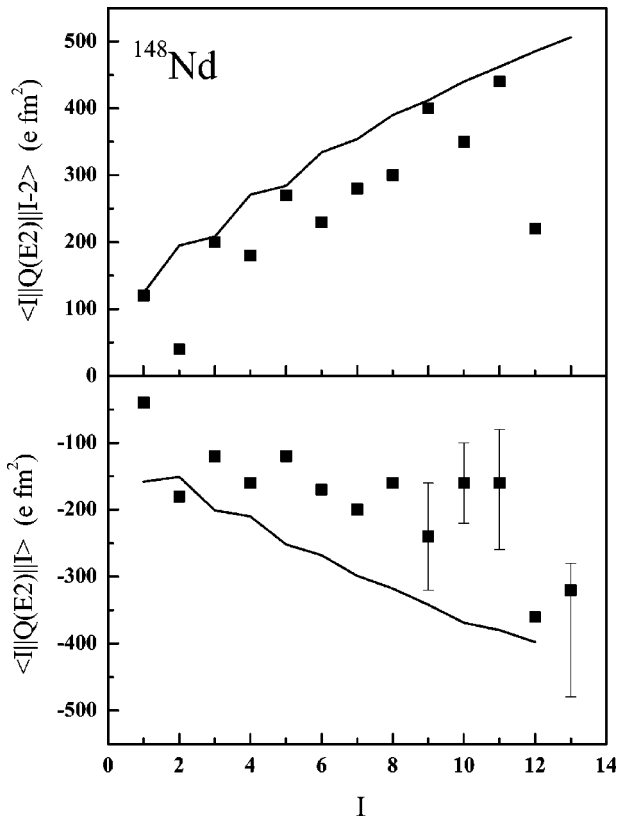

FIG. 8. The same as in Fig. 7, but for the quadrupole operator.

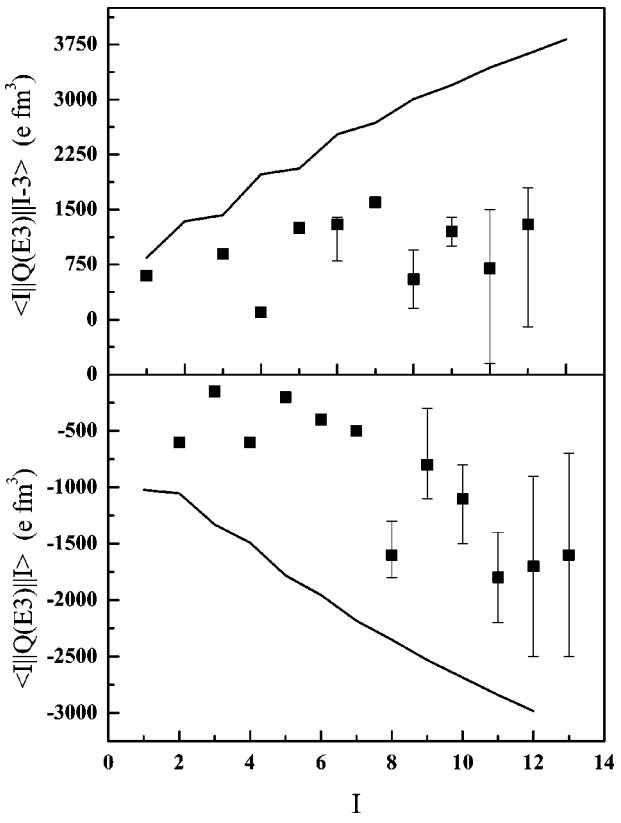

FIG. 9. The same as in Fig. 7, but for the octupole operator.

strikes the barrier, so that the effective coherent tunneling frequency, i.e., the shift of the negative parity states with respect to the positive parity ones, is given by

$$\delta E(I)=\frac{\hbar\omega_m}{\pi}P(I). \tag{A2}$$

Assuming that $[U_b(I=0)-\frac{1}{2}\hbar\omega_m]$ is small compared to $\hbar\omega_b(0)$ (this case is realized in nuclei considered in the paper), we obtain $\hbar\omega_m/2\pi=E(I^\pi=1^-)$. For those values of I at which $U_b(I=0)$ is much smaller than $B_0I(I+1)$ we obtain Eq. (17) with the fitting parameter b_0. However, we found numerically that Eq. (17) works quite well also at low I.

The weight $w_m(I)$ of the mononucleus component in the wave function of the state with spin I can be expressed through the ratio of characteristic times $\tau_m(I)$ and $\tau_b(I)$ which a system spends in the minima and at the barrier, respectively:

$$w_m(I)=\frac{\tau_b(I)}{\tau_b(I)+\tau_m(I)}. \tag{A3}$$

The mononucleus configuration is located at the top of the barrier. We neglect below the I dependence of the $\tau_m(I)$. Denote by $\tau_b(0)$ the value of $\tau_b(I)$ at $I=0$. At very high angular momentum when the barrier height is mainly determined by the rotational energy and is equal to $B_0I(I+1)$ the value of $\tau_b(I)$ can be determined from the time-energy uncertainty relation

$$\tau_b(I\gg 1)=\frac{\hbar}{B_0I(I+1)}. \tag{A4}$$

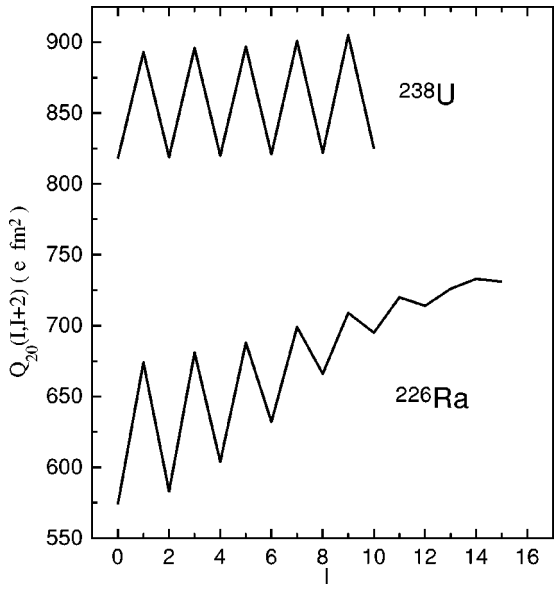

FIG. 10. Angular momentum dependence of calculated intrinsic quadrupole transition moments in ^{226}Ra and ^{238}U.

To combine the two limits at $I=0$ and for $I \gg 1$, we use the following expression:

$$\tau_b(I) = \frac{\hbar}{\hbar/\tau_b(0) + U_b(I) - \hbar\omega_m/2} = \frac{\tau_b(0)}{1+\tau_b(0)B_0 I[I+1]/\hbar}. \tag{A5}$$

Substituting this result into Eq. (A3), we obtain

$$w_m(I) = \frac{\tau_b(0)/(\tau_b(0)+\tau_m)}{1+\frac{\tau_b(0)\tau_m}{\hbar(\tau_b(0)+\tau_m)}B_0 I[I+1]}. \tag{A6}$$

The last expression can be rewritten as

$$w_m(I) = \frac{w_m(0)}{1+b_1 B_0 I(I+1)}, \tag{A7}$$

where $w_m(0) = \tau_b(0)/[\tau_b(0)+\tau_m]$ and $b_1 = (1/\hbar)\tau_b(0)\tau_m/[\tau_m+\tau_b(0)]$.

[1] I. Ahmad and P.A. Butler, Annu. Rev. Nucl. Part. Sci. **43**, 71 (1993).
[2] P.A. Butler and W. Nazarewicz, Rev. Mod. Phys. **68**, 349 (1996).
[3] P. Möller and S.G. Nilsson, Phys. Lett. **31B**, 283 (1970).
[4] G.A. Leander, R.K. Sheline, P. Möller, P. Olanders, I. Ragnarsson, and A.J. Sirk, Nucl. Phys. **A388**, 452 (1982).
[5] A. Sobiczewski and K. Böning, Acta Phys. Pol. B **18**, 393 (1987).
[6] L.M. Robledo, J.L. Egido, J.F. Berger, and M. Girod, Phys. Lett. B **187**, 223 (1987).
[7] F. Iachello and A.D. Jackson, Phys. Lett. **108B**, 151 (1982).
[8] M. Gai *et al.*, Phys. Rev. Lett. **51**, 646 (1983).
[9] H. Daley and F. Iachello, Phys. Lett. **131B**, 281 (1983).
[10] H. Daley and J. Barret, Nucl. Phys. **A449**, 256 (1986).
[11] K. Wildermuth and Y. C. Tang, *A Unified Theory of the Nucleus* (Vieweg, Braunschweig, 1977).
[12] D.A. Bromley, Sci. Am. **239**, 58 (1978).
[13] N. Cindro and W. Greiner, J. Phys. G **9**, L175 (1983).
[14] N.V. Zamfir and D. Kuznezov, Phys. Rev. C **63**, 054306 (1985).
[15] N. V. Zamfir, in *Proceedings of the International Symposium on Nuclear Structure Physics*, edited by R. F. Casten *et al.* (World Scientific, Singapore, 2001).
[16] B. Buck, A.C. Merchant, and S.M. Perez, Phys. Rev. Lett. **76**, 380 (1996).
[17] B. Buck, A.C. Merchant, and S.M. Perez, Phys. Rev. C **58**, 2049 (1998).
[18] B. Buck, A.C. Merchant, and S.M. Perez, Phys. Rev. C **59**, 750 (1999).
[19] B. Buck, A.C. Merchant, and S.M. Perez, Phys. Rev. C **61**, 024314 (2000).
[20] W.D.M. Rae, Int. J. Mod. Phys. A **3**, 1343 (1988).
[21] M. Freer, R.R. Betts, and A.H. Wuosmaa, Nucl. Phys. **A587**, 36 (1995).
[22] M. Freer and A.C. Merchant, J. Phys. G **23**, 261 (1997).
[23] H. Horiuchi, Nucl. Phys. **A552**, 257c (1991).
[24] H. Horiuchi, and Y.K. Kanada-En'yo, Nucl. Phys. **A616**, 394 (1997); Y.K. Kanada-En'yo, Phys. Rev. Lett. **81**, 5291 (1998).
[25] Yu.S. Zamiatin *et al.*, Phys. Part. Nucl. **21**, 537 (1990).
[26] V.V. Pashkevich *et al.*, Nucl. Phys. **A624**, 140 (1997).
[27] S. Aberg and L.O. Jonsson, Z. Phys. A **349**, 205 (1994).
[28] T.M. Shneidman, G.G. Adamian, N.V. Antonenko, S.P. Ivanova, and W. Scheid, Nucl. Phys. **A671**, 119 (2000).
[29] R.V. Jolos, P. von Brentano, and F. Dönau, J. Phys. G **19**, L151 (1993).
[30] R.V. Jolos and P. von Brentano, Phys. Rev. C **49**, R2301 (1994); Nucl. Phys. **A587**, 377 (1995).
[31] T.M. Shneidman, G.G. Adamian, N.V. Antonenko, R.V. Jolos, and W. Scheid, Phys. Lett. B **526**, 322 (2002).
[32] V.V. Volkov, Phys. Rep. **44**, 93 (1978).
[33] G.G. Adamian, A.K. Nasirov, N.V. Antonenko, and R.V. Jolos, Phys. Part. Nucl. **25**, 583 (1994).
[34] G.G. Adamian, N.V. Antonenko, and W. Scheid, Nucl. Phys. **A678**, 24 (2000).
[35] W. Greiner, J. Y. Park, and W. Scheid, *Nuclear Molecules* (World Scientific, Singapore, 1995).
[36] G.G. Adamian *et al.*, Int. J. Mod. Phys. E **5**, 191 (1996).
[37] A. B. Migdal, *Theory of Finite Fermi Systems and Applications to Atomic Nuclei* (Wiley, New York, 1967).
[38] P. Möller *et al.*, At. Data Nucl. Data Tables **59**, 185 (1995).
[39] G.G. Adamian, N.V. Antonenko, and R.V. Jolos, Nucl. Phys. **A584**, 205 (1995).
[40] A. Bohr and B. R. Mottelson, *Nuclear Structure*, (Benjamin, New York, 1975), Vol. II.
[41] http://www.nndc.bnl.gov/nndc/ensdf/
[42] J.F.C. Cocks *et al.*, Nucl. Phys. **A645**, 61 (1999).
[43] I. Wiedenhover *et al.*, Phys. Rev. Lett. **83**, 2143 (1999).
[44] W.R. Phillips, *et al.*, Phys. Rev. Lett. **57**, 3257 (1986).
[45] R. Ibbotson, *et al.*, Phys. Rev. Lett. **71**, 1990 (1993).
[46] W.R. Phillips, *et al.*, Phys. Lett. B **212**, 402 (1988).
[47] W. Urban *et al.*, Phys. Lett. B **200**, 424 (1988).
[48] W. Urban *et al.*, Phys. Lett. B **258**, 293 (1991).
[49] R. Ibbotson, *et al.*, Nucl. Phys. **A530**, 199 (1991).
[50] H. Mach *et al.*, Phys. Rev. C **41**, R2469 (1990).
[51] H.H. Pitz *et al.*, Nucl. Phys. **A509**, 587 (1990).
[52] H.J. Wollersheim *et al.*, Nucl. Phys. **A556**, 261 (1993).
[53] S. Raman *et al.*, At. Data Nucl. Data Tables **36**, 1 (1987).
[54] D. Cline, Nucl. Phys. **A557**, 615c (1993).
[55] L. D. Landau and E. M. Lifschitz, *Quantenmechanik* (Akademie-Verlag, Berlin, 1965), p. 185.